HHS Public Access

Author manuscript

Ophthalmol Retina. Author manuscript; available in PMC 2021 March 01.

Published in final edited form as:

Ophthalmol Retina. 2020 March ; 4(3): 274–283. doi:10.1016/j.oret.2019.10.012.

Lifecycles of individual subretinal drusenoid deposits and evolution of outer retinal atrophy in age-related macular degeneration

Yuhua Zhang, PhD[1,2,*], **Xiaolin Wang, MS**[1], **Srinivas R. Sadda, MD**[1,2], **Mark E. Clark, BS**[3], **C. Douglas Witherspoon, MD**[3], **Richard F. Spaide, MD**[4], **Cynthia Owsley, PhD**[3], **Christine A. Curcio, PhD**[3]

[1]Doheny Eye Institute, 1355 San Pablo Street, Los Angeles, California 90033, USA

[2]Department of Ophthalmology, University of California - Los Angeles, 100 Stein Plaza Driveway, Los Angeles, CA 90024, USA

[3]Department of Ophthalmology and Visual Sciences, University of Alabama at Birmingham, 700 South 18th Street, Birmingham, AL 35294-0009, USA

[4]Vitreous-Retina-Macula Consultants of New York, 460 Park Avenue, 5th Floor, New York, NY 10022, USA

Abstract

Purpose: To describe the progression and regression of individual subretinal drusenoid deposits (SDD) and surrounding photoreceptors and retina in patients with age-related macular degeneration (AMD) over a 3.5-year period, using multimodal imaging including adaptive optics scanning laser ophthalmoscopy (AOSLO).

Design: Longitudinal observational study

Participants: Four patients with intermediate AMD

Methods: Six eyes of 4 patients with intermediate AMD were each imaged 4 times over 3.5 years. Five eyes of 3 patients had only SDD and no drusen. SDD presence and progression were assessed by multimodal imaging and a 3-stage grading system based on spectral domain coherence tomography (SDOCT). Morphology and fine structure of individual SDD lesions identified at baseline were examined by AOSLO at follow-up visits. Reflectivity of photoreceptors surrounding SDD were assessed in AOSLO and SDOCT.

Main Outcome Measures: Morphology, fine structure, and size of individual SDD lesions by AOSLO; photoreceptor integrity surrounding SDD via AOSLO and SDOCT; and retinal layer thicknesses via SDOCT.

[*]**Correspondence and requests for reprints**: Yuhua Zhang, PhD, Doheny Eye Institute, Department of Ophthalmology, University of California - Los Angeles, 1355 San Pablo Street, Los Angeles, California 90033, USA. yzhang@doheny.org.

Results: Individual SDD followed independent lifecycle trajectories, exhibiting growth, shrinkage, fusion, and disappearance. Alterations in shape, morphology, and internal structure were not obviously due to presence of invading phagocytes. Of 822 lesions across all stages examined at baseline, 566 (69%) grew, 123 (15%) shrank, 47 (6%) remained of similar size, 86 (11%) disappeared, and 5 (0.6%) reappeared after regression. A return of characteristic photoreceptor reflectivity in AOSLO (punctate) and in SDOCT (prominent ellipsoid zone) was observed after regression of some SDD in 5 eyes of 4 patients. All eyes exhibited thinning of photoreceptor layers, despite intact RPE, to ~70% of baseline thicknesses, as well as poorly visible or undetectable outer retinal bands.

Conclusions: AOSLO and SDOCT imaging of individual SDD over 3.5 years revealed independent trajectories of progression and regression, believed to reflect the activities of local outer retinal cells. Restoration of some photoreceptor reflectivity and intact RPE after SDD regression should be seen in the larger context of outer retinal atrophy, previously suggested as a new form of advanced AMD, and herein replicated.

INTRODUCTION

Age-related macular degeneration (AMD), which degrades central vision in more than 10 million Americans,[1] is increasingly understood through high-resolution clinical imaging. A layer of extracellular deposits between the retinal pigment epithelium (RPE) and photoreceptors called subretinal drusenoid deposits (SDD; originally called reticular pseudodrusen) were described on optical coherence tomography (OCT) in 2010.[2] Although omitted from AMD staging systems based on color fundus photography (CFP),[3] the presence of SDD is now known to confer risk for progression to late-stage AMD.[4] Further, SDD are associated with accentuated loss of vision, particularly that mediated by rods,[5] relative to eyes with only conventional sub-RPE drusen. Intraretinal (Type 3) neovascularization is associated with SDD, encouraging attention to SDD as a precursor sign.[6]

Far from static, AMD's characteristic extracellular deposits have well defined life cycles that can be visualized almost in their entirety in vivo. This is best demonstrated for soft drusen, the major intraocular risk factor for AMD progression.[3] Soft drusen (medium or larger drusen in grading systems) can be followed through the phases of growth to end-stages of collapse or replacement with fibrotic and crystalline material,[7] as first described in pathology specimens by electron microscopy.[8] These milestones in the progression to atrophy are important both for patient counseling and for designing clinical trials. A detailed understanding of the SDD lifecycle is likely to be similarly informative. Previously, we demonstrated that new-generation adaptive optics scanning laser ophthalmoscopy (AOSLO) together with spectral-domain optical coherence tomography (SDOCT) can disclose individual SDD and surrounding photoreceptors with unprecedented resolution and fidelity.[9] Over a period of 14 months, we observed that individual deposits progressed and then disappeared.[10]

One of us (RFS) described outer retinal atrophy following SDD regression, including outer nuclear layer (ONL) collapse, a poorly visible or non-visible ellipsoid zone (EZ), and a thin

choroid, often with an apparently intact RPE layer.[11] This sequence was proposed as a new form of late stage AMD [11,12] and was distinct from the end stage of geographic atrophy known from CFP to lack continuous RPE.

Further, eyes with SDD only, i.e., lacking drusen but often harboring vitelliform lesions, have been recently described.[13] In this report, we examine individual deposits and outer retinal architecture in eyes with SDD over the same time scale (3.5 years) as the original outer retinal atrophy report,[11] and in several eyes that have only SDD without drusen. We used precisely registered and aligned B-scans, enabling detection and confirmation of this distinctive atrophy. We also simultaneously documented the status of the associated EZ, a marker of photoreceptor integrity. SDD natural history and associated photoreceptor degeneration will be important to consider when elucidating AMD progression and interpreting visual function studies.

METHODS

The study followed the tenets of the Declaration of Helsinki, complied with the Health Insurance Portability and Accountability Act of 1996, and was approved by the Institutional Review Boards at the University of Alabama at Birmingham and the University of California – Los Angeles. Written informed consent was obtained from participants.

Patients:

Patients in an earlier study of SDD microstructure[9] met baseline enrollment criteria of stereotypic reflective material between photoreceptors and RPE on SDOCT that was confirmed with two *en face* modalities. Current study patients were those who continued to meet the criteria below and agreed to return visits. It is worth clarifying that most study eyes had only SDD and had few conventional drusen. When we began patient recruitment in 2010, SDD were called reticular pseudodrusen and had not yet been separated from drusen in SDOCT.[2] Thus these patients were clinically diagnosed with non-neovascular AMD.

Patients diagnosed with AMD were initially recruited from the clinical research registry of the Department of Ophthalmology and Visual Sciences of the University of Alabama at Birmingham and through the Retina Service. All subjects were white of European descent. AMD presence was determined by masked assessment of CFP[14] and clinical record. Exclusion criteria at enrollment were diabetes, history of retinal vascular disease, and any signs or history of hereditary retinal dystrophy. To verify continuing eligibility, stereoscopic digital 30°CFP were taken (FF450 Plus camera, Carl Zeiss Meditec, Dublin, CA) after pupil dilation at every visit. After enrollment, subjects were excluded for reasons that prevented successful imaging, such as poor fixation, significant media opacity, irregular pupil shape, poor dilation, or refractive error beyond ±6 D spherical and ±3 D cylinder. During follow-up, subjects were excluded for the following medical findings in the study eye: neovascularization, geographic atrophy, such as retinal vascular disease (diabetic retinopathy, retinal vein occlusion) or vitreoretinal (vitreomacular traction syndrome, epiretinal membrane) disease. Best-corrected visual acuity (BCVA) was measured by the Electronic Visual Acuity (EVA).[15]

Timeline and study protocol:

Baseline imaging was conducted between February 2012 and August 2015. Follow-up imaging was performed 4 times over 3.5 years. Imaging procedures detailed previously[9] are summarized briefly here.

High-resolution AOSLO image acquisition and process:

The AOSLO is a research system equipped with a custom high-speed Shack-Hartmann wavefront sensor and a high-speed deformable mirror (Hi-Speed DM97–15, ALPAO SAS, France) driven by 97 actuators with stroke up to 30 μm providing improved correction ability for wavefront distortion.[16] It uses a low coherence light source (Broadlighter S840-HP, Superlum, Russia) to reduce light interference artifact. The AOSLO acquires images with a field of view of 1.2° × 1.2° inside the eye at a frame rate of 15 Hz. Before imaging, the subject's pupil was dilated with 1.0% tropicamide and 2.5% phenylephrine hydrochloride. AOSLO videos were recorded continuously across the central 20° × 20°. Registered images were averaged to enhance signal-to-noise ratio. Montages were created with manual cell-to cell alignment (Photoshop, Adobe Systems Inc., Mountain View, CA). AOSLO image pixel size was computed from an image of a precisely calibrated dot grid placed at the retinal plane of a model eye.

Multimodal imaging:

En face near-infrared reflectance (NIR; λ = 830 nm, 30°) images were acquired with a confocal SLO (Spectralis, Heidelberg Engineering, Carlsbad, CA). The retina was imaged cross-sectionally with SDOCT (Spectralis; λ= 870 nm; scan depth, 1.9 mm; axial resolution, 3.5 μm per pixel in tissue; lateral resolution, 14 μm per pixel in tissue). At baseline, 97 B-scans were acquired across the central $15^{o} \times 10^{o}$ area. At follow-up, 194 B-scans were acquired across the central 20°× 20°. We use the OCT band nomenclature of Staurenghi and associates.[17] We also use the term "RPE-basal lamina-BrM" for the fourth outer retinal hyperreflective band, in order to accommodate the appearance of basal laminar deposits in AMD eyes.[18] Multimodal images were precisely registered (Photoshop, Adobe Systems Inc., Mountain View, CA). CFP and SLO NIR images were magnified to match the AOSLO scale (Edit > Transform > Scale), then the SLO NIR and AOSLO images were aligned with CFP using vessels as landmarks (Edit > Transform > Rotate).

SDD identification and classification:

SDD identified at baseline[10] were also examined at each follow-up. Each lesion was scored at each time point with the 3-stage grading system of Zweifel et al.[2] In all patients, both dot and ribbon SDD were discerned. We chose to analyze only dots for comparability with previous studies[19] and also because our imaging instrument did not reveal ribbon SDD distinctly.

Quantifying individual SDD size imaged by AOSLO.

The measurement of SDD size [9,10] is summarized here. At baseline and follow-up, a hyporeflective retinal area associated with each individual SDD was delineated manually and summed using "Polygon Selections" and "Analyze Particles" tools of ImageJ (version

1.50a; http://rsbweb.nih.gov/ij/; National Institutes of Health, Bethesda, MD). For stage 1 and 2 lesions, the affected (hyporeflective) area was measured. For stage 3 lesions, the affected area included a hyporeflective annulus surrounding a hyperreflective center (the deposit). Prior to manual delineation, the borders of hyporeflectivity associated with each individual SDD were enhanced in 2 standardized steps (Photoshop, Adobe Systems Inc., Mountain View, CA). The image was first filtered (Filter > Blur > Gaussian Blur. 'Radius' = 3 pixels), then sharpened (Filter > Sharpen > Smart Sharpen. 'Amount' = 180%, 'Radius' = 64 pixels).

Quantifying SDD impact on overlying retinal structure.

In SDOCT B-scans overlying SDD, we measured thicknesses of inner retina and outer nuclear/Henle fiber layer and the length of photoreceptors. These were measured, respectively, from the inner boundary of the inner limiting membrane (ILM) to the external limiting membrane (ELM), between the outer boundary of the outer plexiform layer (OPL) and the ELM, and between the outer OPL to the midpoint of the RPE. In ImageJ, retinal structure was first enhanced by using the tools 'Brightness and Contrast Adjustment' and 'Filter (Gaussian, 1 pixel).' Then a box with its width equal to the base length of the SDD on the RPE and its height greater than the thickness of the retina-choroid was drawn around the SDD. All thickness parameters were measured within this box. Because photoreceptors overlying the SDD are shortened, photoreceptor length was measured immediately adjacent to the lesion. Each parameter was measured at 3 to 5 points. Mean lengths and standard deviations are reported.

RESULTS

Six eyes of 4 subjects with intermediate stage AMD were studied (Table 1). Five eyes of 3 subjects had only SDD and no drusen over the follow-up period. One eye of one subject had some small hard drusen (< 63 μm) mixed with numerous SDD. A total of 822 SDD lesions across all stages were examined. Of these deposits, 566 (69%) increased in size (by 5.2% - 1233%, from 8,061μm^2 ± 9,699 μm^2 to 15,109 μm^2 ± 13,339 μm^2) over the observation period, 123 (15%) decreased in size (by 5.7% - 87%, from 17,553 μm^2 ± 28,894 μm^2 to 10,778 μm^2 ± 10,640 μm^2), 47 (6%) remained unchanged (≤ 5% difference, from 16,809 μm^2 ± 33,204 μm^2 to 16,960 μm^2 ± 33,167 μm^2), and 86 (11%) disappeared (fully regressed). Five SDD (6%) reappeared after complete regression.

Figure 1 shows CFP of two sets of SDD in patient 1 also shown by AOSLO and OCT in subsequent figures. One set of deposits (arrowheads, Figure 1) are confirmed as SDD with cross-sectional structural OCT in Figure 2. Figure 2 also shows four neighboring deposits following different lifecycle trajectories, i.e., three deposits expand and one contracts. During these phases, SDD morphology also changes, e.g., one deposit acquires hyporeflective divots during growth, and another becomes rectangular during shrinkage.

When viewed *en face,* stage 3 SDD are typically circular with a conical top. This symmetry has face validity considering the precisely spaced photoreceptor outer segments and RPE cells surrounding the deposits.[20] As expected from this orderly environment, Figure 3 shows one deposit with smooth contours (bottom row) that stayed at stage 3 and grew at a steady

pace over 3.5 years. Yet AOSLO also revealed neighboring stage 3 lesions with different shapes and conditions suggesting remodeling as well as regression. Some SDD exhibited growth in concert with reflectivity changes (increase and decrease), triphasic cycles (growth, shrinkage, and growth), fusion, conversion from circular to rhomboid, and appearance of hyporeflective divots and notches within and around the border.

SDD regression and disappearance can be accompanied by return of photoreceptor reflectivity, but in the overall context of outer retinal atrophy, as demonstrated by Figure 4. In general, punctate reflectivity without a contiguous mosaic structure in AOSLO is a non-specific sign requiring further information for identification. For example, punctate reflectivity can represent the internal structure of individual deposits.[9,21] Further, a patterned reflectivity ("pseudo-mosaic") can appear in areas of geographic atrophy, where histology indicates lack of photoreceptors.[22] Thus we examined the area of each regressed deposit via SDOCT to determine if punctate reflectivity in AOSLO was associated with an EZ. Of 86 regressed deposits, 32 (37%) were accompanied by full recovery of the EZ, 11 (13%) with a partially recovered EZ, and 10 (11.6%) with an undetectable EZ; 33 (38%) deposits could not be assessed, because they fell between adjacent SDOCT B-scans. Over the same time, and especially during the last 18 months, the distance between ILM and ELM declined to 51% of baseline levels. Photoreceptor layers thinned, to ~70% of baseline thickness (Figure 4 caption).

Outer retinal atrophy and RPE degeneration associated with SDD regression is shown in Figures 5–6. No sign of atrophy is apparent by CFP (Figure 5). By both AOSLO (Figure 6ABC) and SDOCT (Figure 6D–I) one deposit is seen to disappear over the follow-up period. The RPE is present throughout but is clearly degenerating, because stripes of hypertransmission into the choroid[23] increase in number. Magnified SDOCT scans aligned along the outer border of the RPE-BL-BrM band show an overall shrinkage of retina between ILM and ELM, shrinkage of photoreceptors,[11] and poor visibility of both ELM and EZ. In Figure 6, thicknesses of ILM-ELM, ONL/HFL, and photoreceptors are 90.4%, 60.4%, and 71.2% of thicknesses measured two years prior (details in Figure 6 caption).

DISCUSSION

Using a combination of AOSLO and SDOCT, we examined the fine structure of individual SDD over a period of 3.5 years and observed phases of both progression and regression. Dot form SDD were observed with round, oval, or target shapes[4] with complex morphologies. In general, during growth, dot SDD viewed *en face* have round or oval profiles surrounded by relatively smooth hyporeflective annuli (Figure 2 & 3), consistent with uniform expansion. As SDD regress, the hyporeflective annuli become irregular, indicating non-uniform shrinkage (Figures 2 & 3). By examining details of deposit morphology, we confirmed the previously documented dynamism at 14 months follow-up and additionally sought clues as to contributory factors.

Prior studies in human eyes suggested that the hyporeflective irregularities inside individual SDD might be accounted for by invading phagocytes. Greferath et al in a direct clinicopathologic correlation of stage 3 SDD reported that cells immunoreactive for ionized

calcium binding adaptor molecule 1 (Iba-1), i.e., presumed microglia, appeared in some deposits.[20] However, the smaller deposits of this specimen contained few cells (E.L. Fletcher & U. Greferath personal communication, 6/11/2019), as corroborated by a recent large histologic survey.[24] Paucity of non-local cells is consistent with histologic reports from several laboratories that did not describe or illustrate cells associated with SDD.[8,25–28] In human eyes, subretinal phagocytes clear excess neurons during fetal development,[29,30] and subretinal immune cells are undetectable in normal aged maculas (unpublished observations, n= 60, Project MACULA website; author CAC). These observations in human eyes contrast with those in mouse models,[31,32] in which resident microglia populate the subretinal space, even in aged wild-type animals, and have been interpreted as AMD deposits.[31,32] At our current level of imaging resolution, the independent trajectories of neighboring SDD in these AMD patients do not suggest a role for invading phagocytes but rather, fluctuations in the activity of surrounding outer retinal cells.

The return of photoreceptor reflectivity in 37% of regressed SDD suggests a resumption of waveguiding by realignment or regeneration of outer segments. The phenomenon is unlikely attributable to directional OCT effects due to eye and head positioning,[33] since we checked photoreceptors with both *en face* and cross-sectional imaging. Recent histologic studies have demonstrated new forms of cone photoreceptor degeneration and suggest that under appropriate circumstances, restoration of cone waveguiding may be possible. These include shedding of individual[34] or numerous inner segments[35] at the myoid level. Photoreceptor damage signified by EZ disintegrity, loss, or detachment from the ELM has been shown to be partly [36] or almost completely[35] reversible, if the ELM remains intact. It is too early to determine whether our findings will lend support to ongoing research efforts to rejuvenate photoreceptors, due to the small number of observed deposits overall and the many damaged photoreceptors that accompany widespread SDD. More data to address this critical point are needed. To this end, these study patients are continuing to be followed, to better establish how long these apparently re-constituted photoreceptors can survive.

A larger context for partly restored photoreceptor waveguiding following SDD regression is that it occurs within overall retinal atrophy, as the original findings of Spaide were herein replicated.[11] Figures 4 and 6 show thinning of the ONL over time, so even if with some EZ improvement, these retinas are not healthy, and disease is clearly progressing. Outer retinal architecture and ONL is almost completely lost, and the ELM is discerned only with difficulty. In addition, the choroid is thin and less vascular, and it is likely the choriocapillaris likely is also degenerating. Yet the RPE cells are still present, a feature distinguishing SDD-driven atrophy from drusen-driven atrophy.[37] Despite these changes, BCVA was surprisingly good (20/25 at follow-up). Eyes with SDD have poor rod-mediated vision,[38] suggesting that tests beyond photopic acuity are needed to determine the full functional impact of outer retinal atrophy. Using dark adaptometry, Luu et al reported that rod sensitivity returns, albeit slowly, after a bleaching light, suggesting that photoreceptors are still alive, although dysfunctional.[39]

Strengths of our study include the multi-year observation period, use of *en face* and cross-sectional imaging, and a large sample of individual SDD lesions. The high lateral resolution of AOSLO (2.8 μm, ~1/10th the diameter of smallest SDD detected[9]), the use of the

photoreceptor mosaic as an *en face* reference, and precise alignment of OCT bands provided stage-specific structure and dimensions of lesions[2] and layers more accurately than had we used either B-scan or AOSLO alignment alone. Limitations are the small number of eyes, the restriction to dot lesions, and lack of correlative functional data. Findings in patients with clinical AMD diagnoses and few conventional drusen should be verified in other patient groups. We suspect that any differences found between SDD-bearing eyes with and without drusen will pertain primarily to overall deposit burden. In conclusion, AOSLO imaging combined with SDOCT can reveal in detail altered fine structure of SDD and surrounding photoreceptors over long-term follow-up. Outer retinal atrophy is a late stage of AMD that has recently been considered separate from geographic atrophy, as classically defined in CFP, due to the adoption of SDOCT imaging. Because SDD are now recognized as an important risk factor for vision loss by both atrophic and neovascular progression in AMD, and because they may be an exclusion criterion for therapies that target drusen,[40] improved detection and understanding of SDD merits attention today.

Acknowledgments

Funding/Support: This project was supported by NIH R01EY024378, R21EY027948, R01EY029595, R01AG04212, P30EY003039, and institutional support from Doheny Eye Institute, Research to Prevent Blindness, EyeSight Foundation of Alabama, the Buck Trust of Alabama, the Alfreda J. Schueler Trust, and the Dorsett Davis Discovery Fund. The sponsors or funding organizations had no role in the design or conduct of this research.

Financial Disclosures: No conflicting relationship exists for: Y. Zhang, X. Wang, M. E. Clark, C. D. Witherspoon, C. Owsley. S. R. Sadda receives research funding from Allergan, Carl Zeiss Meditec, Genentech, Optos and Topcon. S. R. Sadda is a consultant for Allergan, Centervue, Genentech, Heidelberg, Iconic, Novartis, Optos, Oxurion; R. F. Spaide is a consultant for Topcon Medical Systems, Genentech, and Roche and receives royalties from Topcon Medical Systems and DORC. C.A. Curcio receives research funding from Heidelberg Engineering and Genentech/Roche.

References

1. Klein R, Chou C-F, Klein BEK, Zhang X, Meuer SM, Saaddine JB. Prevalence of Age-Related Macular Degeneration in the US PopulationPrevalence of AMD in the US Population. JAMA Ophthalmology. 2011;129(1):75–80.
2. Zweifel SA, Spaide RF, Curcio CA, Malek G, Imamura Y. Reticular pseudodrusen are subretinal drusenoid deposits. Ophthalmology. 2010;117(2):303–312 e301. [PubMed: 19815280]
3. Ferris FL 3rd, Wilkinson CP, Bird A, et al. Clinical classification of age-related macular degeneration. Ophthalmology. 2013;120(4):844–851. [PubMed: 23332590]
4. Spaide RF, Ooto S, Curcio CA. Subretinal drusenoid deposits AKA pseudodrusen. Surv Ophthalmol. 2018;63(6):782–815. [PubMed: 29859199]
5. Flamendorf J, Agron E, Wong WT, et al. Impairments in Dark Adaptation Are Associated with Age-Related Macular Degeneration Severity and Reticular Pseudodrusen. Ophthalmology. 2015;122(10):2053–2062. [PubMed: 26253372]
6. Chang YS, Kim JH, Yoo SJ, Lew YJ, Kim J. Fellow-eye neovascularization in unilateral retinal angiomatous proliferation in a Korean population. Acta Ophthalmol. 2016;94(1):e49–53. [PubMed: 25981599]
7. Li M, Dolz-Marco R, Huisingh C, et al. Clinicopathologic Correlation of Geographic Atrophy Secondary to Age-Related Macular Degeneration. Retina. 2019;39(4):802–816. [PubMed: 30839495]
8. Sarks JP, Sarks SH, Killingsworth MC. Evolution of geographic atrophy of the retinal pigment epithelium. Eye (Lond). 1988;2 (Pt 5):552–577. [PubMed: 2476333]

9. Zhang Y, Wang X, Rivero EB, et al. Photoreceptor perturbation around subretinal drusenoid deposits as revealed by adaptive optics scanning laser ophthalmoscopy. Am J Ophthalmol. 2014;158(3):584–596 e581. [PubMed: 24907433]
10. Zhang Y, Wang X, Godara P, et al. Dynamism of Dot Subretinal Drusenoid Deposits in Age-Related Macular Degeneration Demonstrated with Adaptive Optics Imaging. Retina. 2018;38(1):29–38. [PubMed: 28196054]
11. Spaide RF. Outer retinal atrophy after regression of subretinal drusenoid deposits as a newly recognized form of late age-related macular degeneration. Retina. 2013;33(9):1800–1808. [PubMed: 23764969]
12. Spaide RF. Improving the age-related macular degeneration construct: a new classification system. Retina. 2018;38(5):891–899. [PubMed: 28557901]
13. Spaide RF, Yannuzzi L, Freund KB, Mullins R, Stone E. Eyes with subretinal drusenoid deposits and no drusen: progression of macular findings. Retina. 2019;39(1):12–26. [PubMed: 30312263]
14. Davis MD, Gangnon RE, Lee LY, et al. The Age-Related Eye Disease Study severity scale for age-related macular degeneration: AREDS Report No. 17. Archives of ophthalmology. 2005;123(11):1484–1498. [PubMed: 16286610]
15. Beck RW, Moke PS, Turpin AH, et al. A computerized method of visual acuity testing: adaptation of the early treatment of diabetic retinopathy study testing protocol. Am J Ophthalmol. 2003;135(2):194–205. [PubMed: 12566024]
16. Meadway A, Wang X, Curcio CA, Zhang Y. Microstructure of subretinal drusenoid deposits revealed by adaptive optics imaging. Biomed Opt Express. 2014;5(3):713–727. [PubMed: 24688808]
17. Staurenghi G, Sadda S, Chakravarthy U, Spaide RF. Proposed lexicon for anatomic landmarks in normal posterior segment spectral-domain optical coherence tomography: the IN•OCT consensus. Ophthalmology. 2014;doi: 10.1016/j.ophtha.2014.02.023.
18. Balaratnasingam C, Hoang QV, Inoue M, et al. Clinical Characteristics, Choroidal Neovascularization, and Predictors of Visual Outcomes in Acquired Vitelliform Lesions. Am J Ophthalmol. 2016;172:28–38. [PubMed: 27640006]
19. Alten F, Heiduschka P, Clemens CR, Eter N. Longitudinal structure/function analysis in reticular pseudodrusen. Invest Ophthalmol Vis Sci. 2014;55(9):6073–6081. [PubMed: 25146989]
20. Greferath U, Guymer RH, Vessey KA, Brassington K, Fletcher EL. Correlation of Histologic Features with In Vivo Imaging of Reticular Pseudodrusen. Ophthalmology. 2016;123(6):1320–1331. [PubMed: 27039021]
21. Meadway A, Wang X, Curcio CA, Zhang Y. Microstructure of subretinal drusenoid deposits revealed by adaptive optics imaging. Biomedical optics express. 2014;5(3):713–727. [PubMed: 24688808]
22. Paques M, Meimon S, Rossant F, et al. Adaptive optics ophthalmoscopy: Application to age-related macular degeneration and vascular diseases. Progress in retinal and eye research. 2018;66:1–16. [PubMed: 30010022]
23. Xu X, Liu X, Wang X, et al. Retinal Pigment Epithelium Degeneration Associated With Subretinal Drusenoid Deposits in Age-Related Macular Degeneration. Am J Ophthalmol. 2017;175:87–98. [PubMed: 27986424]
24. Chen L, Messinger JD, Zhang Y, Spaide RF, Freund KB, Curcio CA. Subretinal drusenoid deposit in age-related macular degeneration: histologic insights into initiation, progression to atrophy, and imaging. Retina. 2019, doi: 10.1097/iae.0000000000002657.
25. Sarks J, Arnold J, Ho IV, Sarks S, Killingsworth M. Evolution of reticular pseudodrusen. Br J Ophthalmol. 2011;95(7):979–985. [PubMed: 21109695]
26. Rudolf M, Malek G, Messinger JD, Clark ME, Wang L, Curcio CA. Sub-retinal drusenoid deposits in human retina: organization and composition. Exp Eye Res. 2008;87(5):402–408. [PubMed: 18721807]
27. Curcio CA, Messinger JD, Sloan KR, McGwin G, Medeiros NE, Spaide RF. Subretinal drusenoid deposits in non-neovascular age-related macular degeneration: morphology, prevalence, topography, and biogenesis model. Retina. 2013;33(2):265–276. [PubMed: 23266879]

28. Ebrahimi KB, Fijalkowski N, Cano M, Handa JT. Decreased membrane complement regulators in the retinal pigmented epithelium contributes to age-related macular degeneration. The Journal of Pathology. 2013;229(5):729–742. [PubMed: 23097248]
29. McMenamin PG, Loeffler KU. Cells resembling intraventricular macrophages are present in the subretinal space of human foetal eyes. Anat Rec. 1990;227(2):245–253. [PubMed: 2350012]
30. McMenamin PG, Saban DR, Dando SJ. Immune cells in the retina and choroid: Two different tissue environments that require different defenses and surveillance. Prog Retin Eye Res. 2018.
31. Combadiere C, Feumi C, Raoul W, et al. CX3CR1-dependent subretinal microglia cell accumulation is associated with cardinal features of age-related macular degeneration. The Journal of clinical investigation. 2007;117(10):2920–2928. [PubMed: 17909628]
32. Ban N, Lee TJ, Sene A, et al. Impaired monocyte cholesterol clearance initiates age-related retinal degeneration and vision loss. JCI Insight. 2018;3(17).
33. Lujan BJ, Roorda A, Knighton RW, Carroll J. Revealing Henle's fiber layer using spectral domain optical coherence tomography. Invest Ophthalmol Vis Sci. 2011;52(3):1486–1492. [PubMed: 21071737]
34. Litts KM, Messinger JD, Freund KB, Zhang Y, Curcio CA. Inner Segment Remodeling and Mitochondrial Translocation in Cone Photoreceptors in Age-Related Macular Degeneration With Outer Retinal Tubulation. Invest Ophthalmol Vis Sci. 2015;56(4):2243–2253. [PubMed: 25758815]
35. Mehta N, Chong J, Tsui E, et al. Presumed Foveal Bacillary Layer Detachment in a Patient with Toxoplasmosis Chorioretinitis and Pachychoroid Disease. Retinal cases & brief reports. 2018.
36. Wang Q, Tuten WS, Lujan BJ, et al. Adaptive optics microperimetry and OCT images show preserved function and recovery of cone visibility in macular telangiectasia type 2 retinal lesions. Invest Ophthalmol Vis Sci. 2015;56(2):778–786. [PubMed: 25587056]
37. Guymer RH, Rosenfeld PJ, Curcio CA, et al. Incomplete Retinal Pigment Epithelial and Outer Retinal Atrophy (iRORA) in Age-related Macular Degeneration: CAM Report 4. Ophthalmology. 2019.
38. Chen KG, Alvarez JA, Yazdanie M, et al. Longitudinal Study of Dark Adaptation as a Functional Outcome Measure for Age-Related Macular Degeneration. Ophthalmology. 2019;126(6):856–865. [PubMed: 30278196]
39. Luu CD, Tan R, Caruso E, Fletcher EL, Lamb TD, Guymer RH. Topographic Rod Recovery Profiles after a Prolonged Dark Adaptation in Subjects with Reticular Pseudodrusen. Ophthalmology Retina. 2018;2(12): 1206–1217. [PubMed: 31047193]
40. Guymer RH, Wu Z, Hodgson LAB, et al. Subthreshold Nanosecond Laser Intervention in Age-Related Macular Degeneration: The LEAD Randomized Controlled Clinical Trial. Ophthalmology. 2019;126(6):829–838. [PubMed: 30244144]

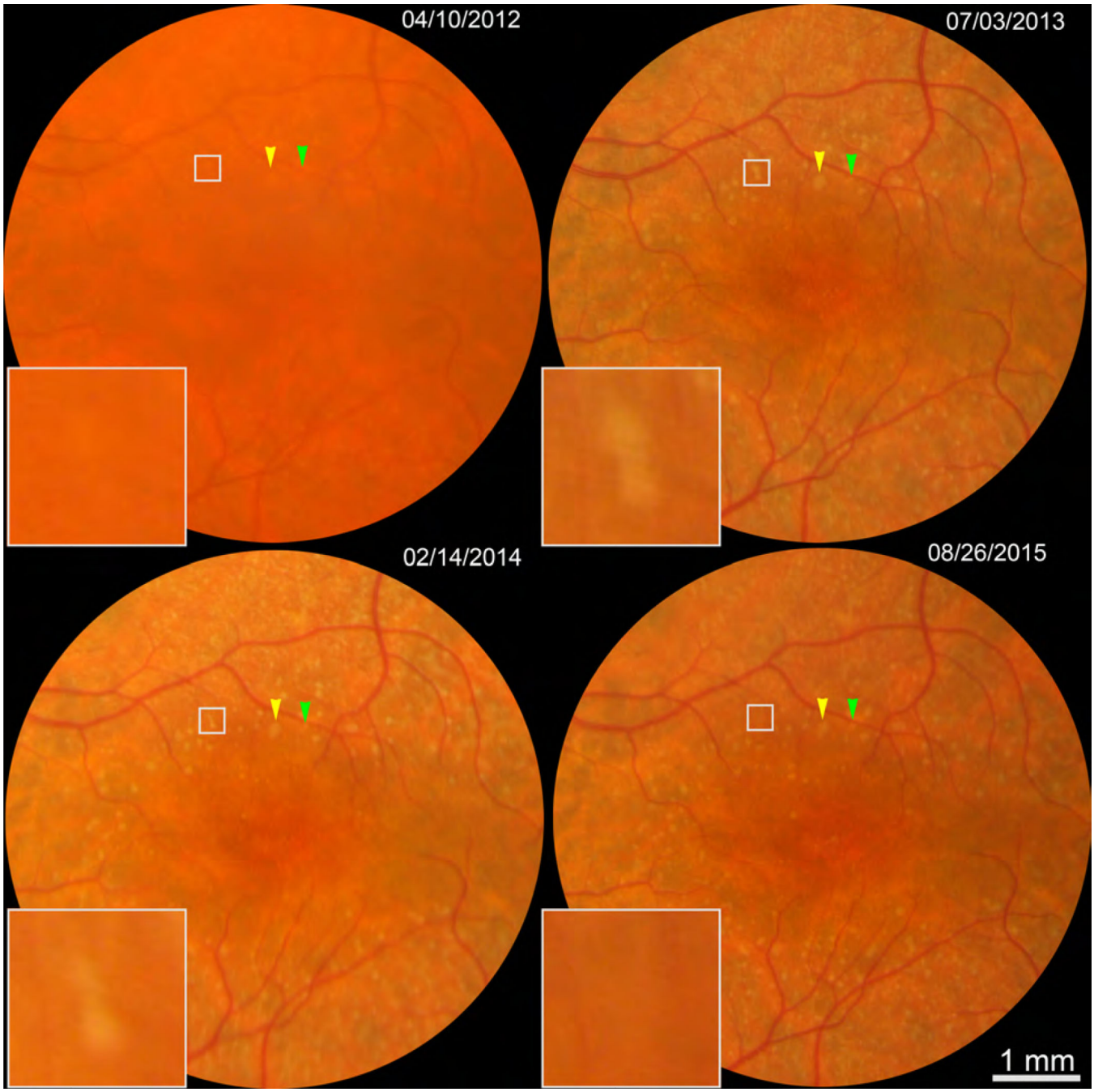

Figure 1.

Color fundus photography of subretinal drusenoid deposits (SDD) in one patient over 3.5 years. Color arrowheads indicate 2 SDD detailed in Figure 2. White boxes show 2 regressing SDD detailed in Figure 4. This is the left eye of Patient 1 in Table 1, who had surgery removing cataract after the 1st visit.

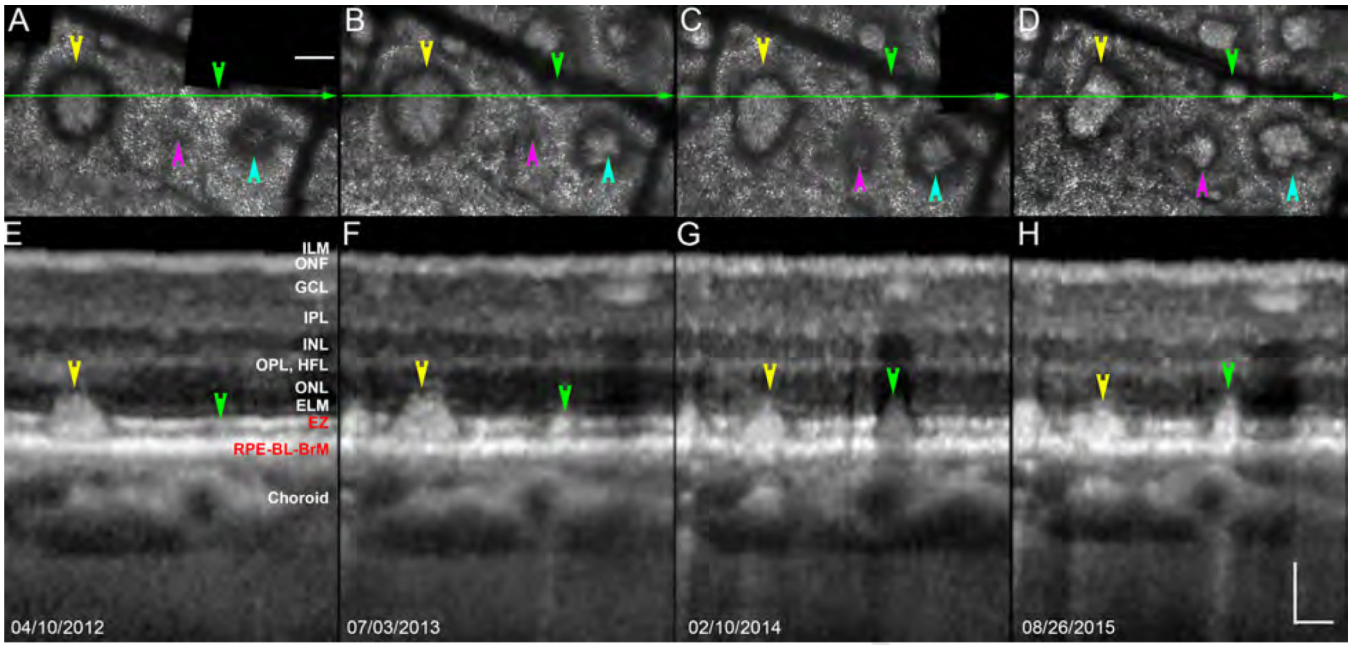

Figure 2.

Neighboring subretinal drusenoid deposits exhibit a range of dynamic processes. A - D are AOSLO images of the subject shown in Figure 1, at the same 4 follow-up dates. OCT images were acquired at a position represented by the green line. Over 3.5 years, some deposits grow (magenta, green, and teal arrowheads) and others shrink (yellow arrowhead). Deposit morphology can change during both phases (teal, acquiring divots during growth, and yellow, becoming rectangular during shrinkage). Adaptive optics scanning laser ophthalmoscopy (top row) and spectral-domain optical coherence tomography (bottom row). Patient 1 in Table 1. ILM: Internal limiting membrane, which is the inner noundary of the ONF. ONF: Optic nerve fibers. GCL: Ganglion cell layer. IPL: Inner plexiform layer. INL; Inner nuclear layer. OPL: Outer plexiform layer. HFL: Henle Fiber layer. ELM: External limiting membrane. EZ: elipsoid zone. RPE: retinal pigment epithelium. BL: basal lamina. BrM: Bruch's membrane. The RPE-BL-BrM band includes the hyperreflective RPE, hyporeflective basal laminar deposit, and hyperreflective BrM. Due to space limitations, the entire complex is labeled together in panel E. Scale bar = 100 μm.

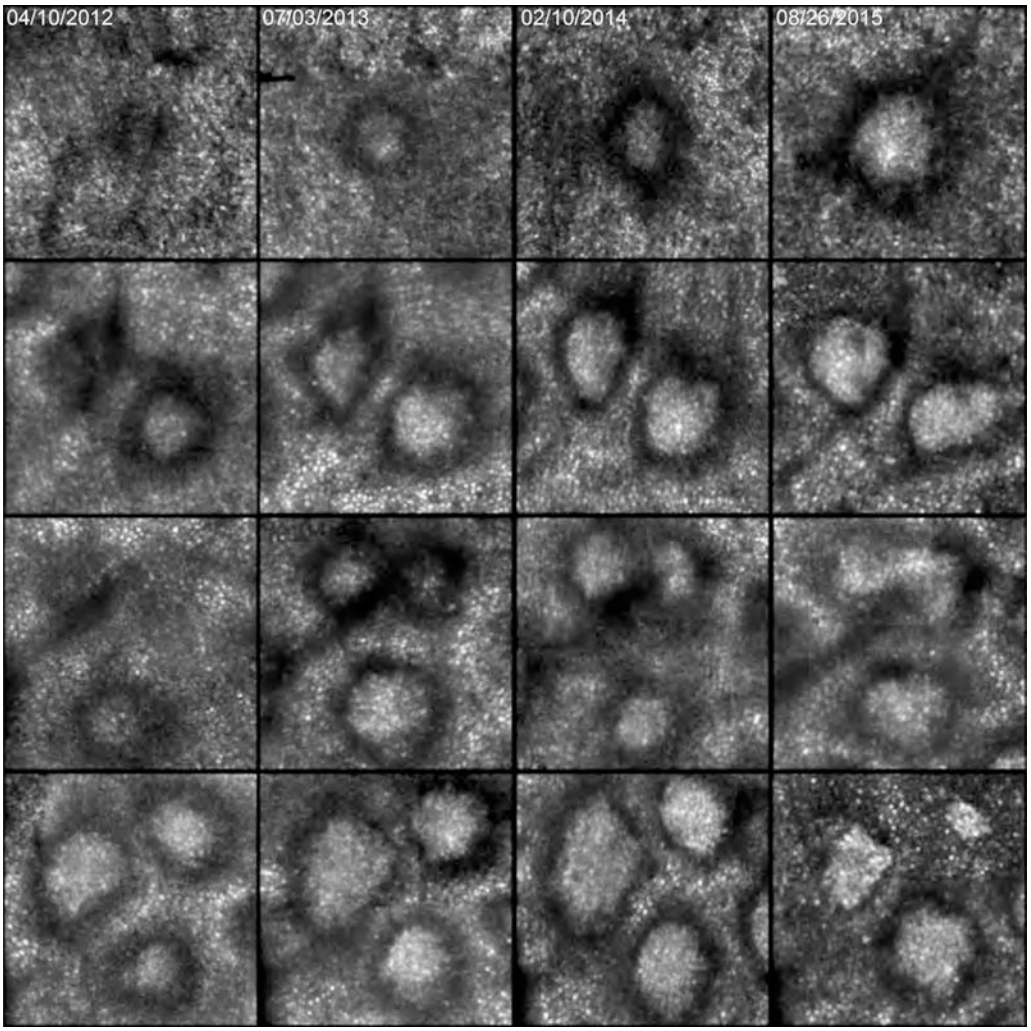

Figure 3.

Progression of individual subretinal drusenoid deposit (SDD) over 3.5 years seen in adaptive optics scanning laser ophthalmoscopy. Each row represents 1 degree (300 μm) inside the eye, imaged on the dates shown at the top of each column. Top row: one deposit grows and gains reflectivity. Second row: of two deposits, the top one starts at stage 2, grows, becomes stage 3, gaining reflectivity overall but losing reflectivity at divot-like regions. The bottom deposit starts at stage 3 with a wide annulus, and the center slightly elongates. Third row, two deposits at the top appear on slightly different time frames, then fuse. A deposit at the bottom grows to 15 months, shrinks, then grows again. Fourth row: the top left and right deposits grow and change from circular to rhomboid at 22 months, then shrink and gain reflectivity at 3.5 years. The deposit at the bottom stays at stage 3 and grows smoothly. Patient 1 in Table 1.

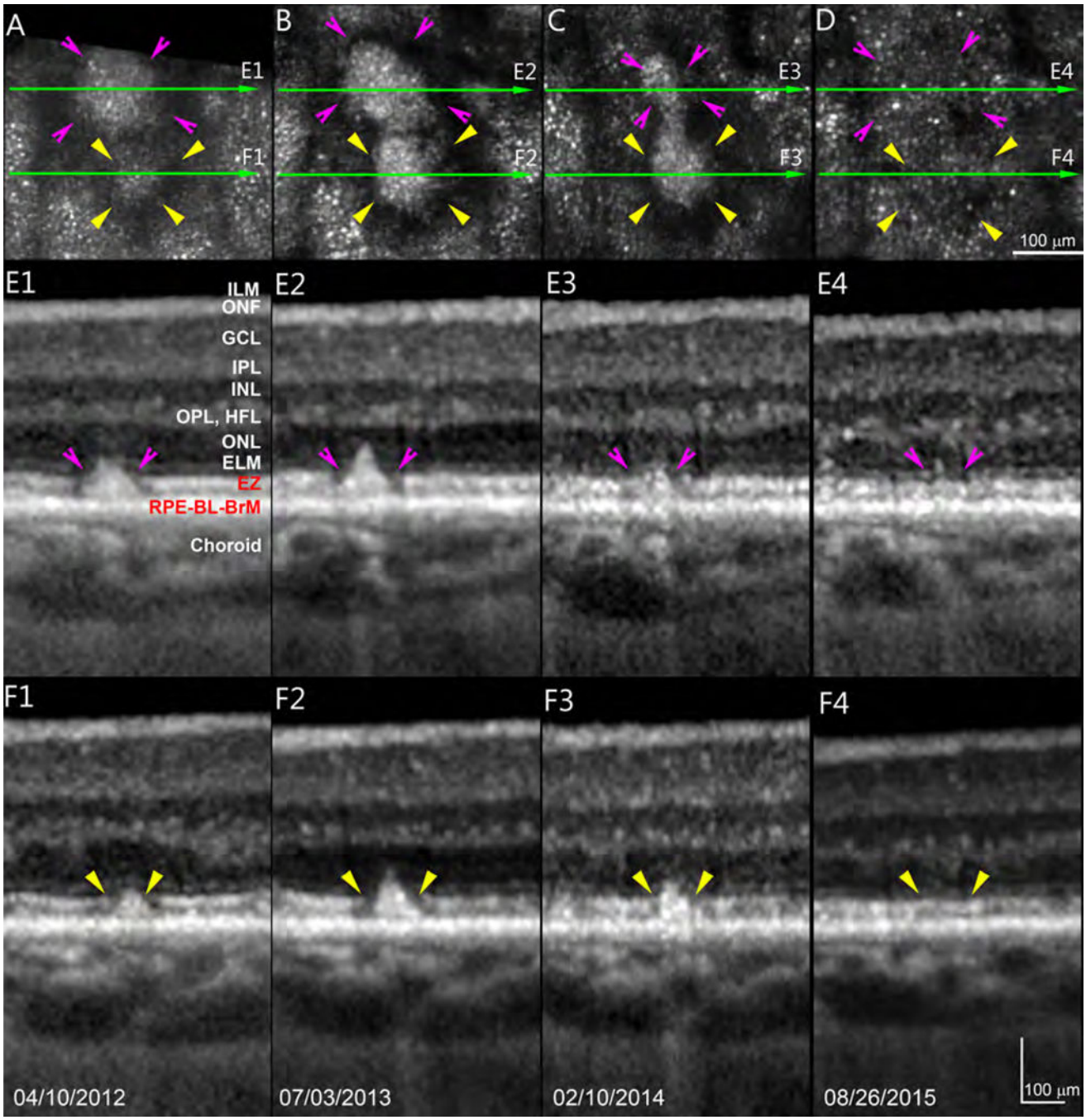

Figure 4.

Photoreceptor reflectivity restoration and retinal thinning after regression of subretinal drusenoid deposits. Two deposits indicated by pink and yellow arrowheads are observed over 3.5 years in Patient 1 at sites shown in Figure 1 (white boxes). Green arrow-lines indicate spectral-domain optical coherence tomography (OCT) B-scans shown in panels E1-E4 and F1-F4. A punctate reflectivity (panel D) by adaptive optics scanning laser ophthalmoscopy corresponds to a nearly intact ellipsoid zone by OCT (E4,F4). In Panels E1 – E4, distances from ILM to ELM are (respectively) 253, 244, 244, and 235 μm.

Thicknesses of ONL/Henle fiber layer are 58, 48, 41, 30 μm. Photoreceptor length was defined as the outer portion of the OPL to the middle point of RPE.[11] Lengths in E1 – E4 are 130, 122, 122, and 97 μm. After SDD regression, thicknesses of ONL/Henle fiber layer of E4 is 51.7% that of E1, photoreceptor length of E4 is 74.6% of that E1. In Panels F1 – F4, distances from ILM to ELM are (respectively) 254, 249, 241, and 226 μm. Thicknesses of ONL/Henle fiber layer are 56, 53, 47, 29 μm. Photoreceptor lengths are 130, 122, 112, and 88 μm. After SDD regression, thicknesses of ONL/Henle fiber layer of F4 is 51.8% that of F1, whereas photoreceptor length of F4 is 67.7% of that F1. ILM: Internal limiting membrane, which is the inner boundary of the ONF. ONF: optic nerve fibers. GCL: Ganglion cell layer. IPL: Inner plexiform layer. INL; Inner nuclear layer. OPL: Outer plexiform layer. HFL: Henle Fiber layer. ELM: External limiting membrane. EZ: elipsoid zone. RPE: retinal pigment epithelium. BL: basal lamina. BrM: Bruch's membrane. The RPE-BL-BrM band includes the hyperreflective RPE, hyporeflective basal laminar deposit, and hyperreflective BrM. Due to space limitations, the entire complex is labeled together in panel E1. Scale bars represent 100 μm.

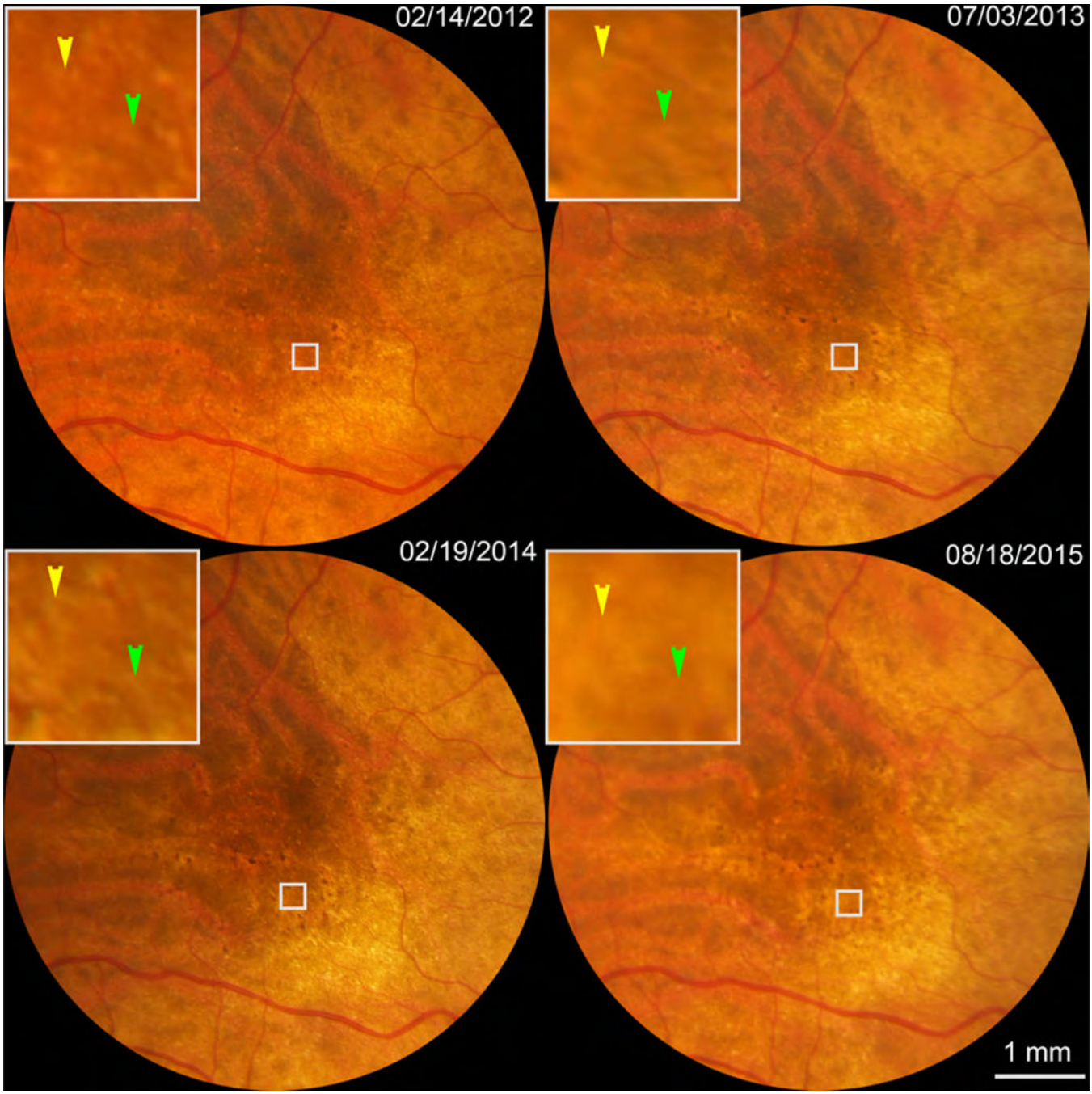

Figure 5.

Color fundus photography of an eye exhibiting outer retinal atrophy associated with regression of subretinal drusenoid deposits (SDD). White boxes show 2 regressing SDD (indicated by color arrowheads) that are detailed in Figure 6. This is the right eye of Patient 2 in Table 1.

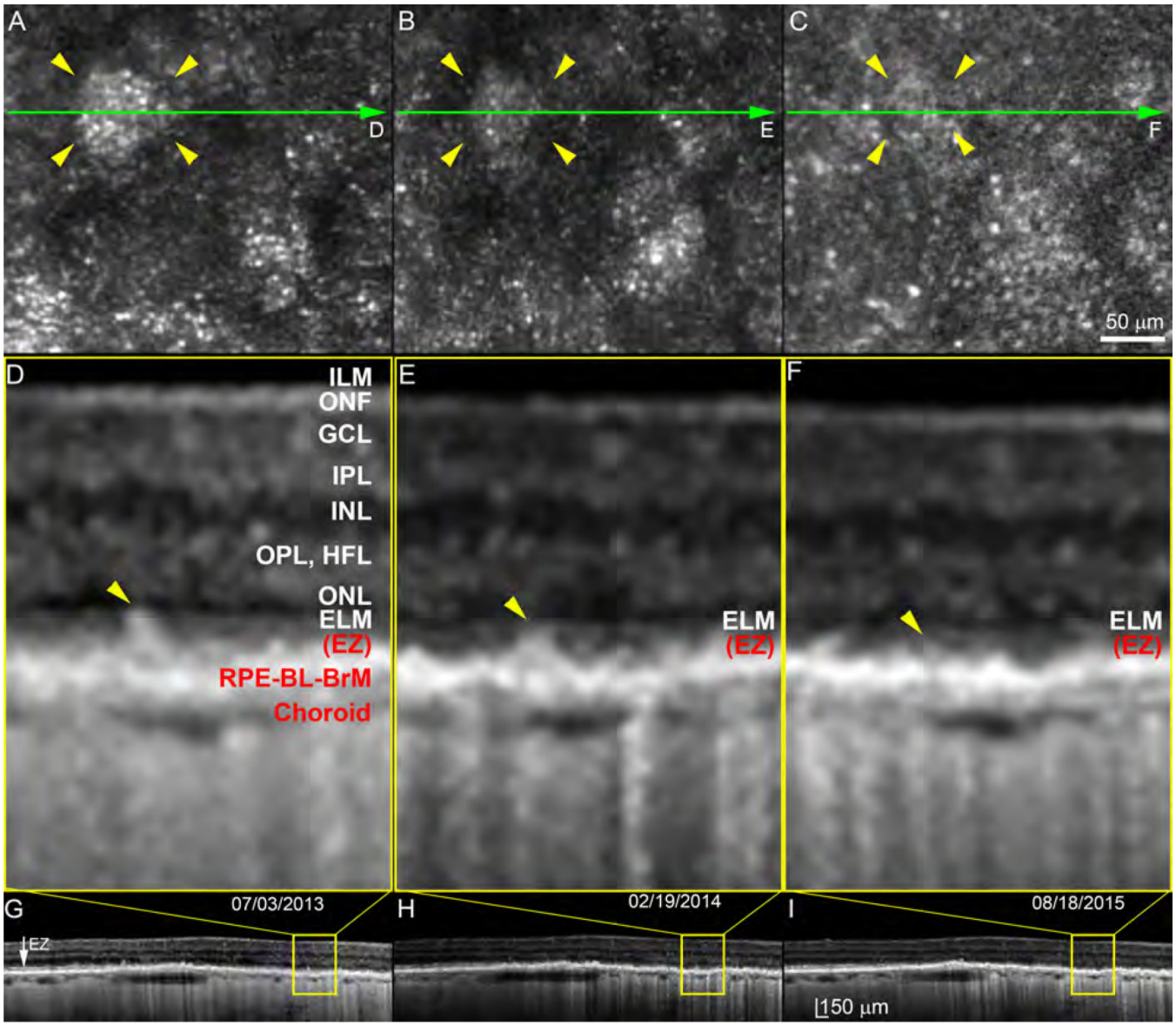

Figure 6.

Outer retinal atrophy and retinal pigment epithelium degeneration associated with subretinal drusenoid deposit regression. This patient was followed for 3.5 years by adaptive optics scanning laser ophthalmoscopy (see white boxes in Figure 5), which showed loss of both deposit reflectivity and the annulus representing deflected photoreceptors. Spectral-domain optical coherence tomography revealed an almost complete loss of the outer retinal architecture. Yellow arrowheads point to the regresseed SDD. In Panels DEF, distances from ILM to ELM are (respectively) 199, 191, and 180 μm. Thicknesses of ONL/HFL are 43, 34, and 26 μm. Photoreceptor lengths, defined as the outer portion of the OPL to the middle point of RPE,[11] were 66, 54, and 47 μm. Thus thicknesses of ILM-ELM, ONL/HFL, and photoreceptors are 90.4%, 60.4%, and 71.2% of thicknesses two years prior. The ELM becomes less visible over time. The EZ is not clear at any time point. RPE cells are still present, but streaks of hypertransmission into the choroid indicate patchy RPE degeneration.

The choroid is thin and has low vascularity at all time points. ILM: Internal limiting membrane, which is the inner boundary of the ONF. ONF: Optic nerve fibers. GCL: Ganglion cell layer. IPL: Inner plexiform layer. INL; Inner nuclear layer. OPL: Outer plexiform layer. HFL: Henle Fiber layer. ELM: External limiting membrane. EZ: elipsoid zone. RPE: retinal pigment epithelium. BL: basal lamina. BrM: Bruch's membrane. The RPE-BL-BrM band includes the hyperreflective RPE, hyporeflective basal laminar deposit, and hyperreflective BrM. Due to space limitations, the entire complex is labeled together in panel D. As EZ has lost its continuity due to atrophy, we labeled EZ with brackets indicating its position. The scale bar in panel C applies for panels A and B. The scale bar in panel I also applies for panels G and H.

Table 1:

Summary of study patient characteristics

Patient	Age at baseline	Gender	Study Eye		Lesion presence		Follow-up (Months)	Visual acuity	
			OS	OD	SDD	Drusen		Baseline	End Visit
1	73	Male	Y*	N	Y(OU)	N(OU)	39	20/25(OS)*	20/16(OS)
2	84	Female	Y	Y	Y(OU)	N(OU)	42	20/50(OS)	20/63(OS)
								20/16(OD)	20/25(OD)
3	78	Female	Y	Y	Y(OU)	N(OU)	42	20/63(OS)	20/63(OS)
								20/50(OD)	20/40(OD)
4	76	Female	Y	N†	Y(OU)	Y(OU)	34	20/25(OS)	20/25(OS)

*Patient had surgery removing cataract after the 1st visit. The fellow eye (OD) had neovascular AMD.

†OD had thick cataract and small pupils.